Interfacial Redox Catalysis on Gold Nanofilms at Soft Interfaces

Evgeny Smirnov,[†] Pekka Peljo,[†] Micheál D. Scanlon,[†,‡] and Hubert H. Girault*[,†]

[†]Laboratoire d'Electrochimie Physique et Analytique, Ecole Polytechnique Fédérale de Lausanne, Station 6, CH-1015 Lausanne, Switzerland and [‡]Department of Chemistry and the Tyndall National Institute, University College Cork, Cork, Ireland

ABSTRACT Soft or "liquid–liquid" interfaces were functionalized by roughly half a monolayer of mirror-like nanofilms of gold nanoparticles using a precise interfacial microinjection method. The surface coverage of the nanofilm was characterized by ion transfer voltammetry. These gold nanoparticle films represent an ideal model system for studying both the thermodynamic and kinetic aspects of interfacial redox catalysis. The electric polarization of these soft interfaces is easily controllable, and thus the Fermi level of the electrons in the interfacial gold nanoparticle film can be easily manipulated. Here, we study interfacial redox catalysis between two redox couples located in adjacent immiscible phases and highlight the catalytic properties of a gold nanoparticle film toward heterogeneous electron transfer reactions.

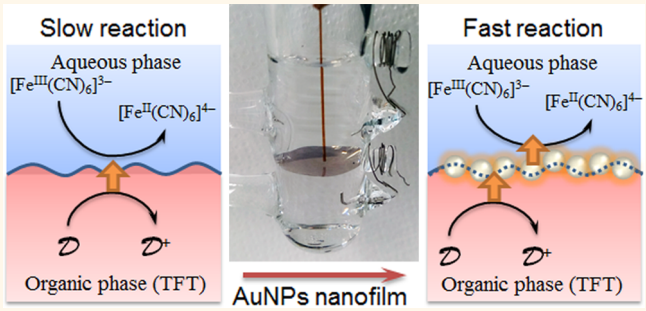

KEYWORDS: gold nanoparticles · Fermi level equilibration · liquid–liquid interfaces · redox catalysis · electron transfer · nanofilm

Polarizable soft interfaces between two immiscible electrolyte solutions (ITIES) have emerged as model platforms at which to study charge transfer reactions that impact energy research, chiefly the hydrogen evolution (HER)[1−5] and oxygen reduction reaction (ORR).[6−11] Soft interfaces also represent an ideal system at which to self-assemble molecules or nanoparticles (NPs) into 2D films that are defect-free, are mechanically flexible, and exhibit self-recovery.[12,13] A variety of functionalized soft interfaces have been realized by the self-assembly of supramolecular arrays,[8] noble metallic NPs,[14−16] magnetic particles such as Fe_2O_3,[17] and quantum dots.[18] Energy-related reactions may be favored by soft interfaces functionalized with either molecular adsorbed catalytic species, such as porphyrins,[6,7] or solid nanoparticles, such as MoS_2 for the HER[4] or Pt[9] and reduced graphene oxide[10] for the ORR. Often, the role of the adsorbed interfacial species is to accept and store electrons from a molecular donor in the organic phase, relay them to an electron acceptor, and provide a binding site for reactive intermediates.

Functionalization of soft interfaces with self-assembled films of gold NPs (AuNPs) is an area of avid research for technological applications ranging from optics (flexible mirrors and filters),[16,19] to sensors,[20,21] to biomedical research (size-selective dialysis membranes and drug-delivery capsules),[22] to catalysis,[23] *etc.* Several methods exist to induce the self-assembly of AuNPs at soft interfaces. Since Reincke and co-workers[24] reported the spontaneous self-assembly of AuNPs at a water | heptane interface following the addition of alcohol, numerous alternative approaches have been described to trigger the assembly of metallic NPs at soft interfaces.[15,25,26] The alcohol injection method is still one of the most convenient but requires introducing a substantial volume of alcohol (at least 10 vol %)[27−29] close to the interface and lacks a precise control of the interfacial surface coverage of AuNPs in the film.

The redox properties of metallic NPs, and by extension their self-assembled 2D films, depend directly, but not exclusively, on the excess charge present on the metallic NP.[30] The latter may be either electronic or due to the presence of adsorbed ionic species or ligands. However, adsorbed neutral ligands also influence the redox properties of metallic NPs by altering their surface potential.[30]

The Fermi level of the electrons in metallic NPs (E_F^{NP}), such as AuNPs, depends first on their synthesis route, then on their

* Address correspondence to Hubert.Girault@epfl.ch.

Received for review April 28, 2015 and accepted June 3, 2015.

Published online June 03, 2015
10.1021/acsnano.5b02547

conservation method (aerobic *versus* anaerobic) but most crucially on their environment.[30] When AuNPs are placed into a solution containing a redox couple (Ox/Red) in excess, E_F^{NP} equalizes with the Fermi level of the electrons in solution for this redox couple, which is given directly by the Nernst equation. For the AuNPs to attain the Fermi level imposed by the redox couple, an electrochemical reaction should take place to charge the AuNPs either negatively, raising E_F^{NP}, or positively, lowering E_F^{NP}. Similarly, if AuNPs are in contact with a solution of, for example, ferri/ferrocyanide in excess, E_F^{NP} is given by the Nernst equation for this redox couple and may be manipulated by varying the relative concentrations of the two species (ferri/ferro).

When more than one redox couple is present in a solution, a thermodynamic equilibrium should be reached between all redox couples. However, due to kinetic limitations, the system may remain out of equilibrium. In this instance, the addition of colloidal NPs can catalyze Fermi level equilibration in solution, and this process is called redox catalysis.[31,32] Another scenario involves having two different redox couples present in separate immiscible phases, for example, ferri/ferrocyanide in the aqueous phase and ferrocenium/ferrocene in the adjacent organic phase. At equilibrium, the Fermi levels of the electrons in both phases are aligned, but analogous to homogeneous systems, equilibrium may not be reached due to kinetic limitations. Indeed, such is the case for the decamethylferrocenium/decamethylferrocene (organic phase) and $2H^+/H_2$ (aqueous phase) redox couples, even at high positive polarization of the aqueous phase with respect to organic phase.[33] Adsorption of a suitable catalyst at the liquid−liquid interface can significantly enhance the reaction rates, thereby achieving interfacial redox catalysis at functionalized soft interfaces.[34]

It is important to note that soft interfaces are polarizable and therefore offer an additional parameter to control the position of equilibrium: the Galvani potential difference across the interface ($\Delta_o^w\phi$).[35] The flow of current across the interface to reach a new equilibrium can be manipulated or even reversed in direction by adjusting $\Delta_o^w\phi$, and such reactions may be catalyzed by NPs adsorbed at the soft interface. These abilities identify polarizable functionalized soft interfaces as an excellent model system to study interfacial redox catalysis at adsorbed species.

Heterogeneous electron transfer (HET) reactions at the ITIES are known to be potential dependent, *i.e.*, dependent on the interfacial polarization, but it is difficult to evaluate how much of the overall polarization is active as a local driving force. In the early days, these reactions were thought to take place solely by true heterogeneous electron transfer (ET), as suggested by Samec *et al.*[36] for the system comprising $K_{3/4}[Fe(CN)_6]$ in water and ferrocene in the organic phase, meaning that an aqueous redox couple is supposed to react with an organic redox species only at the interface where ET reactions occur. However, it was then postulated, *e.g.*, by Kihara *et al.*,[37] Osakai *et al.*,[38] and Katano *et al.*,[39] that one of the reactants can in fact partition to undergo a homogeneous ET, with associated ion transfer (IT) reactions, and that the current measured was not always due to a heterogeneous ET but rather to the preceding or following IT reaction.

Herein, we introduce a reproducible and precise method of functionalizing soft interfaces with one nanoparticle thick gold nanofilms using an interfacial microinjection method. Subsequently, we provide an in-depth characterization of the interfacial redox catalysis between ferri/ferrocyanide in the aqueous phase and ferrocenium/ferrocene in the organic phase at an adsorbed AuNP film by comparison of voltammetry and finite element simulations. A theoretical description of the observed processes in terms of Fermi level equilibration is presented as a general model for understanding interfacial redox catalysis.

RESULTS AND DISCUSSION

Fermi Level Equilibration and the Kinetics of Electron Transfer across the Soft Interface. Let us consider a heterogeneous redox reaction between an aqueous redox couple O_1/R_1 and an organic redox couple O_2/R_2:

$$n_2O_1^w + n_1R_2^o \rightleftarrows n_2R_1^w + n_1O_2^o \quad (1)$$

where n_1 and n_2 are the number of electrons exchanged for each redox couple. At equilibrium, the Fermi level of the electrons in water (E_F^w) is equal to that in the organic phase (E_F^o), as illustrated in Scheme 1. E_F^w is given by the Nernst equation and the Galvani potential of water on the absolute vacuum scale (AVS) taking the electron at rest under vacuum as the origin (in kJ mol^{-1}):

$$E_F^w = -F\left[[E^0_{O_1/R_1}]^w_{SHE} + \frac{RT}{n_1F}\ln\left(\frac{c^w_{O_1}}{c^w_{R_1}}\right) + \phi_w + [E^0_{H^+/1/2H_2}]^w_{AVS}\right] \quad (2)$$

where $[E_{H^+/(1/2)H_2}{}^0]^w_{AVS}$ = 4.44 V is the potential of the standard hydrogen electrode (SHE) on the absolute vacuum scale and $\phi_w = \chi_w + \psi_w$ is the Galvani potential (also called the inner potential) of the aqueous phase, where χ_w is the surface potential and ψ_w is the outer potential of the aqueous phase. Unfortunately, it is not possible to measure the Galvani potential of a phase, so the absolute value of E_F^w is not known. However, it is possible to measure the Galvani potential difference between the aqueous and organic phases. Similarly, E_F^o is given by

$$E_F^o = -F\left[[E^0_{O_2/R_2}]^o_{SHE} + \frac{RT}{n_2F}\ln\left(\frac{c^o_{O_2}}{c^o_{R_2}}\right) + \phi_o + [E^0_{H^+/1/2H_2}]^w_{AVS}\right] \quad (3)$$

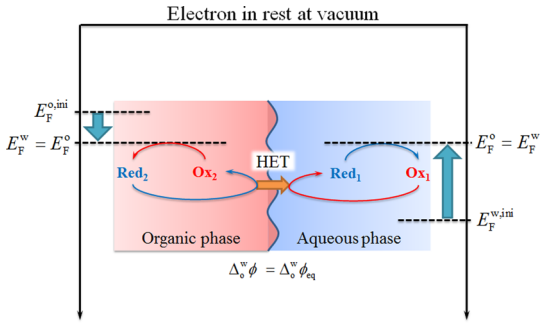

Scheme 1. Equilibration of the Fermi level of the electrons in water (E_F^w) with electrons in the organic phase (E_F^o) *via* heterogeneous electron transfer (HET) across the soft interface. The positions of E_F^w and E_F^o are represented under conditions where thermodynamic equilibrium is reached between both redox couples in the adjacent phases (*i.e.*, no kinetic limitations to Fermi level equilibration are present). $E_F^{w,ini}$ and $E_F^{o,ini}$ are the initial Fermi levels of aqueous (blue) and organic (red) phases, respectively (see text for additional details).

where ϕ_o is the Galvani potential of the organic phase.

The equilibrium Galvani potential difference $\Delta_o^w\phi_{eq}$ is defined as

$$[\phi_w - \phi_o]_{eq} = \Delta_o^w\phi_{eq} = [E_{O_2/R_2}]_{SHE}^o - [E_{O_1/R_1}]_{SHE}^w = \Delta_o^w\phi_{HET}^0 + \frac{RT}{n_1n_2F}\ln\left(\frac{c_{R_1}^w}{c_{O_1}^w}\right)^{n_2}\left(\frac{c_{O_2}^o}{c_{R_2}^o}\right)^{n_1} \quad (4)$$

with $\Delta_o^w\phi_{HET}^0$, the standard Galvani potential difference for the heterogeneous electron transfer (HET), given by

$$\Delta_o^w\phi_{HET}^0 = [E_{O_2/R_2}^0]_{SHE}^o - [E_{O_1/R_1}^0]_{SHE}^w \quad (5)$$

Thus, by polarizing the soft interface, we can change the potential of the organic redox couple (and also E_F^o) *with respect to* the aqueous redox couple; now the concentration ratios of $[O_2^o]/[R_2^o]$ and $[O_1^w]/[R_1^w]$ will adjust so that equilibrium is attained once more. $\Delta_o^w\phi$ may be adjusted by an external power supply.

Let us now discuss the scenario when a metallic NP is adsorbed at the soft interface and in contact with two redox couples. If the latter are not in equilibrium, a mixed potential is established such that both the oxidation and reduction half-reactions proceed at the same rate on the surface of the metallic NP. We can consider the half-reactions

$$O_1 + n_1e^{-NP} \underset{k_{-1}}{\overset{k_1}{\rightleftharpoons}} R_1 \quad (6)$$

$$R_2 \underset{k_{-2}}{\overset{k_2}{\rightleftharpoons}} O_2 + n_2e^{-NP} \quad (7)$$

where reduction (eq 6) and oxidation (eq 7) take place at the aqueous and organic sides of the interface, respectively, with the metallic NP acting as a bipolar electrode. The rates of both electrochemical reactions can be considered to follow a Butler–Volmer formalism using Fermi levels in solids and solutions instead of electrode potentials. These rates are governed by an exponential term dependent on the difference between the Fermi levels of the electrons in solution and the electrons in the metal (E_F^{NP}), *i.e.*, the driving force, the rate constant k^0, which is driving force independent, and the surface concentrations of reacting species.

If we assume that back-reactions are negligible, the current i_1 for the reduction half-reaction (eq 6) is

$$i_1 = -n_1A_1Fk_1^0c_{O_1}^{w,s}e^{(1-\alpha_1)n_1(E_F^{NP}-E_F^w)/RT} \quad (8)$$

where k_1^0 is the potential-independent rate constant, A_1 is the area available for reaction 6 being either that of a single NP or of an "island" of electronically interacting NPs, α_1 is the charge transfer coefficient (commonly close to 0.5), and $c_{O_1}^{w,s}$ is the surface concentration of O_1 in the aqueous phase. Note that the oxidative current is defined as positive, in accordance with IUPAC definitions, and the Fermi level of electrons in solutions is expressed as defined in eqs 2 and 3.

Correspondingly, for the oxidation half-reaction (eq 7),

$$i_2 = n_2A_2Fk_2^0c_{R_2}^{o,s}e^{-\alpha_2n_2(E_F^{NP}-E_F^o)/RT} \quad (9)$$

Note that the terms E_F^o and E_F^w contain the Galvani potentials for both phases. Additionally, as ET takes place from a higher into a lower Fermi level, we have $E_F^w < E_F^o$.

For floating metallic NPs in solution, the current for both reactions is the same, so $i_1 = -i_2$ (*i.e.*, a key assumption is that the metallic NP is chemically inert in solution). Hence, at a steady state, E_F^{NP} is controlled by the ratio of the two rate constants:

$$E_F^{NP} = \frac{((1-\alpha_1)n_1E_F^w + \alpha_2n_2E_F^o)}{((1-\alpha_1)n_1 + \alpha_2n_2)} - \frac{RT}{((1-\alpha_1)n_1 + \alpha_2n_2)}\ln\left[\frac{n_1A_1k_1^0c_{O_1}^{w,s}}{n_2A_2k_2^0c_{R_2}^{o,s}}\right] \quad (10)$$

If back-reactions cannot be neglected, the situation becomes too complicated to be easily solved analytically, and numerical methods are required.

The influence of the different relationships between $A_1k_1^0$ and $A_2k_2^0$ on the position of E_F^{NP} is illustrated in Scheme 2. For example, if $\alpha_1 = \alpha_2 = 0.5$, $n_1 = n_2 = n$, and the concentrations of O_1/R_1 and O_2/R_2 are similar, then eq 10 simplifies to

$$E_F^{NP} = \frac{(E_F^w + E_F^o)}{2} - \frac{RT}{n}\ln\left[\frac{A_1k_1^0c_{O_1}^{w,s}}{A_2k_2^0c_{R_2}^{o,s}}\right] \quad (11)$$

If $A_1k_1^0$ and $A_2k_2^0$ are equal, and if the number of transferred electrons (n_1 and n_2) is also equal, then the position of E_F^{NP} (a turquoise line) is half of the sum of the Fermi levels of the two redox couples (Scheme 2B).

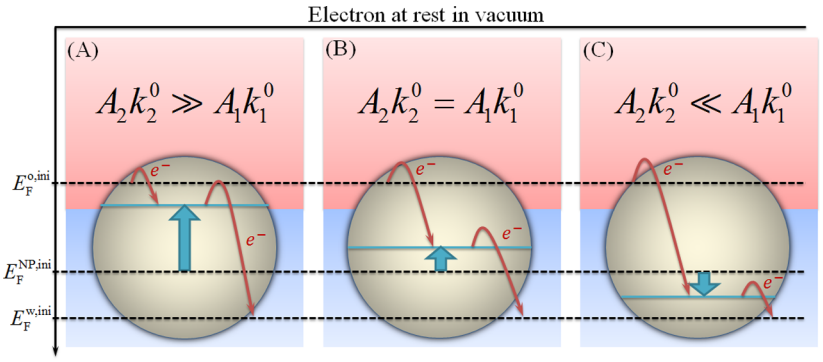

Scheme 2. Interfacial redox catalysis: equilibration of the Fermi level of the electrons in a metallic NP (E_F^{NP}) adsorbed at a soft interface and in contact with two redox couples, one in the aqueous phase (1) and the other in the organic phase (2). The final position of E_F^{NP} (a turquoise line) is determined by the kinetics of both the oxidation and reduction half-reactions (eqs 6 and 7 in the text): (A) $A_2k_2^0 \gg A_1k_1^0$, (B) $A_2k_2^0 = A_1k_1^0$, and (C) $A_2k_2^0 \ll A_1k_1^0$. Limitations of this approach: the metallic NP is chemically inert in the solution and interacts with the redox couples; also the concentration of the redox couples is the same at any point in the solution (no mass transfer limitations).

However, if $A_2k_2^0 \gg A_1k_1^0$, additional driving force (overpotential) is required to drive the reduction half-reaction (eq 6) at the same rate as the oxidation half-reaction (eq 7). Note that ET occurs from E_F^o to E_F^w, so $E_F^w < E_F^o$. This results in equilibration of E_F^{NP} closer to E_F^o (Scheme 2A). In this scenario, the metallic NP is often termed a "reservoir of electrons" as the NP is charged with electrons to increase E_F^{NP}. Similarly, if $A_2k_2^0 \ll A_1k_1^0$, additional overpotential is required to conduct the oxidation half-reaction at the same speed as the reduction half-reaction, and, thus, equilibration is reached when E_F^{NP} is closer to E_F^w (Scheme 2C). In this case, the metallic NP is called a "reservoir of holes".

As noted in the introduction, if one redox couple is dominating, E_F^{NP} is pinned by the redox potential of that couple. Thus, if one redox couple is present in significant excess compared to the other (and the kinetics are reasonably facile), E_F^{NP} adjusts close to the redox potential of that couple. The Fermi level of electrons in the NP will always be found between E_F^w and E_F^o.

Finally, by polarizing the metallic NP functionalized soft interface (*i.e.*, establishing a new value of $\Delta_o^w\phi_{eq}$), we also change the difference between E_F^w and E_F^o (see eqs 2−4). For example, if E_F^{NP} is pinned by an aqueous redox couple, changing $\Delta_o^w\phi_{eq}$ by +0.5 V will lower E_F^o by −0.5 eV with respect to E_F^{NP}. This change will trigger ET until a new equilibrium is reached (in effect the surface concentration ratios of $c_{O_2}^{o,s}/c_{R_2}^{o,s}$ and $c_{O_1}^{w,s}/c_{R_1}^{w,s}$ adjust to the new $\Delta_o^w\phi_{eq}$). If E_F^{NP} is exactly between E_F^w and E_F^o, changing $\Delta_o^w\phi_{eq}$ will affect the overpotentials for both reactions equally. The gap between E_F^w and E_F^o changes or even inverts, but E_F^{NP} will remain in the middle. Finally, it is also worth noting that this theoretical approach is equally applicable to homogeneous redox catalysis reactions, where both reactions take place in a single phase *i* with a Galvani potential ϕ_i.

Functionalization of Soft Interfaces with Mirror-like AuNP Nanofilms. An interfacial microinjection approach has been developed to deliver AuNPs to the interface and to considerably improve the control of the AuNP surface coverage in comparison with previously reported methods. The process involves three steps: (i) synthesis of citrate-stabilized AuNPs, (ii) concentration of these AuNPs by centrifugation and resuspension of the concentrate in methanol, and (iii) precisely controlled injection of the methanol-suspended AuNPs at a soft water | trifluorotoluene (TFT) interface using a capillary and a syringe-pump to deliver a small volume of the methanol solution of AuNPs (Figure 1A). Previously, Park and co-workers used a syringe-pump to carefully inject pure ethanol at a water | hexane interface but without preconcentrating the AuNPs in alcohol. Larger quantities of alcohol (milliliter *versus* microliter volumes used here) were required to achieve mirror-like AuNP films.[28]

Interfacial AuNP nanofilms were formed with either 12 or 38 nm mean diameter AuNPs. The mean diameters of the as-synthesized citrate-stabilized AuNPs were determined by characterization with transmission electron microscopy (TEM), UV/vis spectroscopy, and dynamic light-scattering (DLS) measurements; see the Supporting Information, SI-1. As depicted in Figure 1B to D, the methanol-suspended AuNPs were injected at the interface at a controlled rate of 10 μL/min.

The injected AuNPs immediately assembled into one nanoparticle thick isolated gray islands floating at the interface, each island gradually increasing in size with continued AuNP injection. The interface was slightly perturbed by the flow from the capillary, and, thus, each AuNP island was constantly in motion. Eventually, all of the individual islands of AuNPs coalesced to form a dense mirror-like AuNP nanofilm. For the four-electrode electrochemical cells illustrated in Figure 1B and C, 10 μL of concentrated 12 nm AuNPs

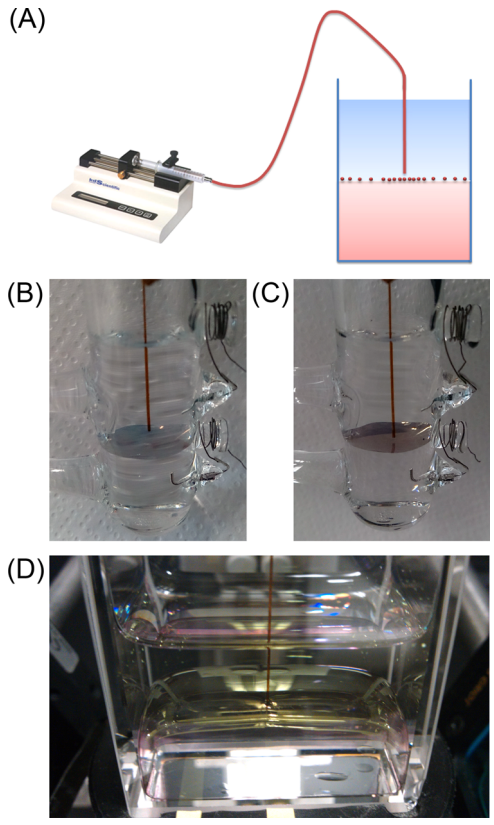

Figure 1. Functionalization of soft interfaces with AuNP nanofilms by precise injection of AuNPs suspended in methanol at the interface. (A) Schematic of the capillary and syringe-pump setup used to settle AuNPs directly at the interface between two immiscible liquids allowing precise control over the AuNP surface coverage. Examples of AuNP films prepared at flat soft water | trifluorotoluene interfaces in four-electrode electrochemical cells using AuNPs with mean diameters of (B) 12 nm and (C) 38 nm. Flat soft interfaces were achieved by partial silanization of the bottom half of the electrochemical cell glass walls. (D) AuNP nanofilms were also prepared on larger curved soft interfaces using a 2 × 4 cm quartz cell.

and 20 μL of 38 nm AuNPs in methanol were required to cover the flat 2.5 cm^2 water | TFT soft interface. Typically, water | oil interfaces in hydrophilic glassware are curved due to differences in surface tension between the organic solvent, water, and glass itself. An important aspect of this work was to determine the surface coverage of AuNPs as accurately as possible. To achieve the latter, flat interfaces with well-defined surface areas were preferred and realized by partial silanization of the electrochemical cell. The nanofilm formation process for the larger 38 nm AuNPs was recorded with time using a ProScope HD USB-microscope, and each step is clearly illustrated in the Supporting Information, SI-2.

All of the AuNPs injected into the electrochemical cell were retained at the soft interface; the latter can be seen in Figure 1B and C as clean, transparent, and noncolorized solutions below and above the settled nanofilm. Thus, as the interfacial area, the concentration of the AuNPs in the methanol solution, and the volume of AuNPs injected (controlled by the flow-rate and injection time period) were precisely known, an accurate control of the surface coverage of AuNPs was possible, as shown previously.[16] The precision of the method is mostly limited by the determination of the bulk AuNP concentration using Haiss and co-workers methodology based on UV−vis spectra[40] and can be estimated as 5−7% of standard deviation. By this method, nanofilms of half a monolayer were prepared, with the surface coverage estimated from the hexagonal packing as 37%.

Additionally, the presented method is scalable, appropriate for flat (Figure 1B and C) or curved (Figure 1D) soft interfaces, and generally applicable to other immiscible water | oil combinations, such as water | 1,2-dichloroethane, water | 1,2-dichloromethane, and water | nitrobenzene.

Ion Transfer Voltammetry Characterization of AuNP Nanofilm Functionalized Soft Interfaces. Packing arrangements of the AuNPs at the soft interface were investigated by carefully transferring the interfacial 38 nm AuNP film to a silicon substrate and characterizing it with scanning electron microscopy (SEM). Settling of the AuNPs leads to partial occupation of the interface by a one nanoparticle thick nanofilm (submonolayer), which can be distributed in two ways: (i) randomly, forming a continuous network on NPs with voids in between, or (ii) in an island-like manner, where hexagonally closed packed islands coexist with voids of the same dimensions (Figure 2C). In fact, the preparation method results in films that are a combination of both morphologies: randomly distributed network of NPs with voids of different sizes, small and big ones (see Supporting Information SI-3). Thus, in effect, the AuNP nanofilm patterns the soft interface with a randomly distributed array of micropores, and the theory of voltammetry on partially blocked electrodes[41] can be applied for any ion transfer (IT) reactions. Amatore and co-workers introduced the concept of a zone diagram for various types of blockage, depending on morphology, size, and interparticle distance (or distance between blocking compounds). Recently, this topic has been reviewed by Davies and Compton.[42] If the diffusion zone radius (δ) is larger than both pore center-to-center distance (S) and pore radius (r), in the so-called heavily overlapping diffusion zones condition, mass transfer occurs by apparent semilinear diffusion from the bulk and a classical peak-shaped cyclic voltammogram (CV) is obtained (Figure 2B and D).

First, CVs with only background electrolytes present in the absence and presence of AuNP nanofilms consisting of either 12 or 38 nm AuNPs were obtained using electrochemical cell 1 outlined in Scheme 4B of the Methods section. CVs with well-defined potential windows of *ca.* 1 V width, limited by the IT of Cl^- at the negative potentials and Li^+ at positive potentials, were attained in all cases (Figure 2A). In

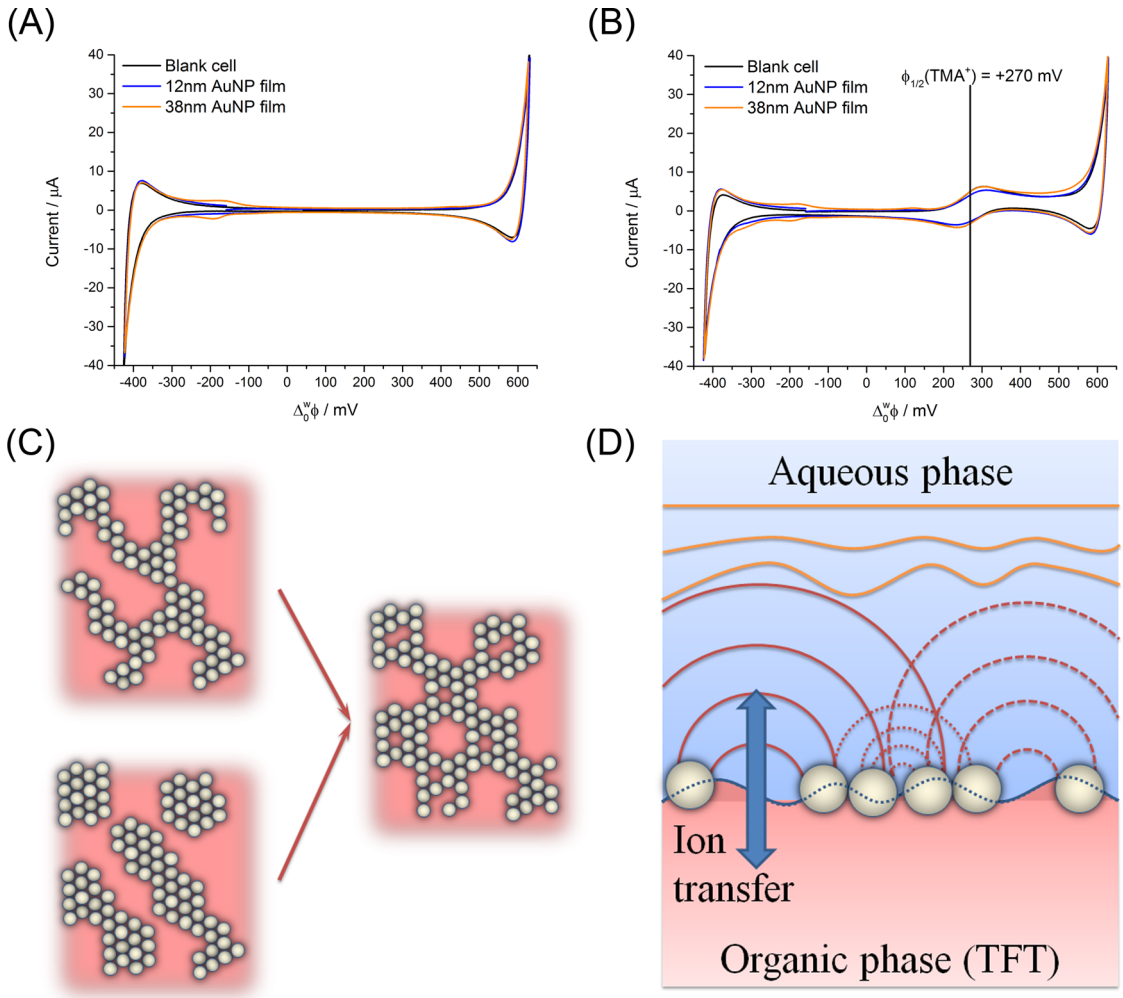

Figure 2. Cyclic voltammetry (CV; *IR* compensated) at bare and AuNP nanofilm modified soft interfaces formed between a 10 mM LiCl aqueous solution and a 5 mM BATB solution in TFT. CVs were obtained at a scan rate of 25 mV/s (A) without and (B) with TMA^+ ions present for calibration. (C) Schematic representation of possible distribution of AuNPs in the nanofilm at ITIES: randomly distributed network (top), islands with voids (bottom), and mixed morphology (middle). (D) Schematic representation of the cross-sectional view of the ITIES partially occupied by a nanofilm of AuNPs (lines show the diffusion profiles of ion concentration).

marked contrast to previous reports,[27,29] no decrease of the window and lowering of the Gibbs energies of transfer of the aqueous background electrolyte ions in the presence of the AuNP nanofilms were observed. This is attributed to the significantly lower volumes of methanol required to achieve the dense mirror-like film formation here than reported in previous studies. Thus, IT and ET events of interest taking place at potentials close to the transfer of the background electrolyte ions may now be observed in the presence of an interfacial AuNP nanofilm. Control experiments, summarized in the Supporting Information section SI-4, show that methanol, sodium citrate, and ascorbic acid with concentrations at least an order of magnitude higher than those used in the AuNP nanofilm preparation did not significantly affect the CVs.

Next, CVs were obtained in the presence of the non-redox-active tetramethylammonium cation, TMA^+, in the aqueous phase. The presence of the interfacial AuNP nanofilms did not significantly alter the voltammetric response for TMA^+ transfer, in accordance with previously published results,[27,29] with clear peak-shaped responses obtained on both the forward and reverse sweeps (Figure 2B). This indicates that the diffusion zones between individual micropores were heavily overlapping, as illustrated in Figure 2C and D.

Scan-rate analysis using the Randles-Ševčík equation[43] allows the determination of the percentage of the surface covered by AuNPs (see Supporting Information SI-4B). In the presence of an interfacial AuNP nanofilm consisting of either 12 or 38 nm AuNPs, respectively, the nanofilm coverage was estimated to be about 30%. This value corresponds roughly to half a hexagonal close packed monolayer (surface coverage of 37%), considering that 70% of the surface area is available for semi-infinite linear diffusion. According to the blocked electrode theory, the apparent

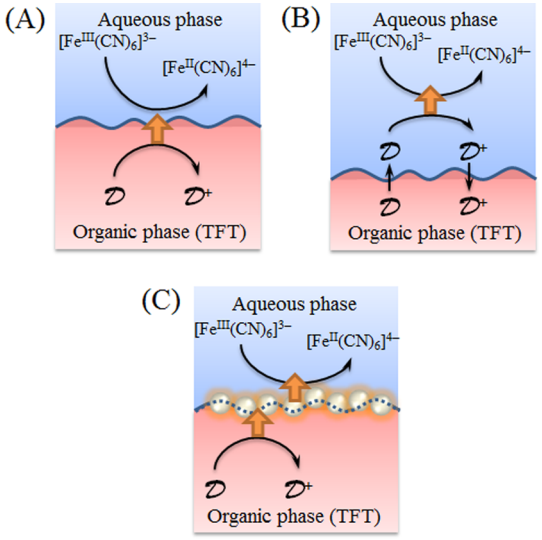

Scheme 3. Possible mechanisms, each leading to measurable current across the polarized soft interface as described in the main text, when an electron donor species ($\mathcal{D}$) is present in the organic phase and an electron acceptor species (such as ferri/ferrocyanide) is present in the aqueous phase: (A) bimolecular heterogeneous electron transfer, (B) a homogeneous electron transfer−ion transfer mechanism, and (C) interfacial redox catalysis with the AuNP nanofilm acting as a bipolar electrode. The orange arrow indicates the electron transfer reaction with a rate constant k^0.

IT rate should decrease with increasing surface coverage (θ_{AuNP}) of the blocking particles ($k^0_{IT,app} = k^0_{IT}(1 - \theta_{AuNP})$).[41] However, herein the IT reactions still exhibited reversibility and were not disturbed by a 30% surface coverage of the blocking layer (Figure 2B).

Interfacial Redox Catalysis at a Polarized AuNP Nanofilm Functionalized Soft Interface. ET across the AuNP film functionalized soft interface was examined using a model system, namely, the electron donor redox couple $Fc^{+/0}$ dissolved in the organic phase and the electron acceptor redox couple $[Fe(CN)_6]^{3-/4-}$ dissolved in the water phase.[36,38,39] At bare (without AuNP nanofilm) soft interfaces, an ET reaction involving this model system can proceed in two ways: (i) bimolecular heterogeneous ET (HET), between $[Fe(CN)_6]^{3-/4-}$ in water and $Fc^{+/0}$ in oil, as suggested by Samec *et al.* and described in eq 12 (Scheme 3A):[36]

$$[Fe(CN)_6]^{3-}(w) + Fc^0(o) \rightleftarrows [Fe(CN)_6]^{4-}(w) + Fc^+(o) \quad (12)$$

or (ii) a homogeneous ET-IT mechanism involving partition of neutral Fc^0 into the water phase, followed by homogeneous ET with $[Fe(CN)_6]^{3-}$ and subsequent IT of Fc^+ back to the organic phase, as postulated by the groups of Kihara,[37] Osakai,[38] and Katano[39] (Scheme 3B). As we will show in a separate publication, the two mechanisms occur concomitantly, and the observed experimental current is a combination of HET and ET−IT processes.

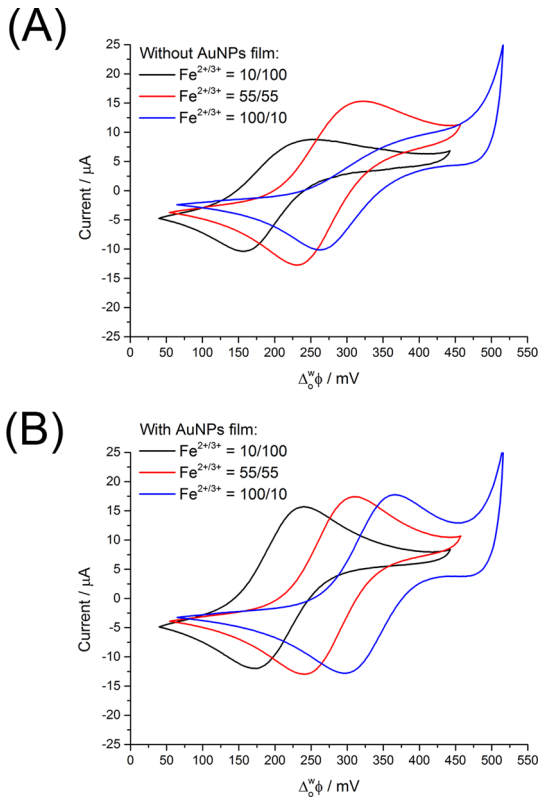

Figure 3. Experimental evidence of interfacial redox catalysis in the presence of the AuNP nanofilm. Cyclic voltammograms (*IR* compensated) of ET between the oil-solubilized $Fc^{+/0}$ redox couple and the aqueous $[Fe(CN)_6]^{3-/4-}$ redox couple, with various ratios between Fe^{2+} and Fe^{3+} investigated, both (A) in the absence and (B) in the presence of a AuNP nanofilm at the soft interface. All electrochemical cells were prepared as described in Scheme 4B. Scan rate: 10 mV s^{-1}.

At AuNP nanofilm functionalized soft interfaces, the ET reaction preferably takes place on the bipolar film, where the Fermi level on the AuNPs is fixed by the aqueous redox couple in excess acting as an electrode to oxidize the ferrocene in the organic phase eqs 13 and 14:

$$NP^{ze} + [Fe(CN)_6]^{3-}(w) \rightleftarrows NP^{(z-1)e} + [Fe(CN)_6]^{4-}(w) \quad (13)$$

$$NP^{ze} + Fc^0(o) \rightleftarrows NP^{(z+1)e} + Fc^+(o) \quad (14)$$

where z represents the charge number on the core of the AuNP. This process is called interfacial redox catalysis and is illustrated in Scheme 3C.[44]

A comparison of experimental CVs in both the absence and presence of the AuNP nanofilms is shown in Figure 3A and B, with various ratios of $[Fe(CN)_6]^{3-/4-}$ (see Scheme 4B in the Methods section for the compositions of the investigated electrochemical cells). ET appears reversible under semi-infinite linear diffusion control when the nanofilm is present, providing clear evidence that the nanofilm acts as an efficient redox catalyst, despite a low surface coverage of *ca.* 30% of

the gold island. As summarized in Table 1, in the absence of the nanofilm the peak-to-peak separation for ET (ΔE_p) was 90 mV or above for the three $Fe^{2+/3+}$ ratios investigated, whereas with the nanofilm present ΔE_p was between 65 and 70 mV even when *IR* compensation was utilized to eliminate most of the contributions from ohmic drop in the system. Additionally, the ratio of forward and reverse peak currents i_{pf}/i_{pb} is closer to unity in the presence of the nanofilm (Table 1).

According to the partially blocked electrode theory, the reaction kinetics appear more irreversible (larger separation of the peak potentials) with practically no effect on the peak currents with increasing coverage of the blocking layer. Utilizing the method of Nicholson (see the Supporting Information, SI-4C, for further details), the experimental peak separation of 66 mV indicates that *ca*. one-fifth of the interface is active for interfacial electron transfer, in agreement with the surface coverage estimated theoretically from the AuNP concentration (37%) and from the IT experiments (*ca*. 30%).

The observed voltammetry in Figure 3A and B can be understood by the theory presented above. At a bare soft interface, initially no noticeable ET takes place, indicating that E_F^o is lower than E_F^w. As $\Delta_o^w\phi$ is scanned to more positive potentials, at a certain point E_F^o rises above E_F^w, driving ET from oil to water (positive current). When the sweep direction is reversed, the Fermi levels invert to drive ET from water to oil (negative current).

At AuNP nanofilm modified soft interfaces, the nanofilm can be treated as a bipolar electrode. If the back-reactions are neglected, E_F^{NP} of the nanofilm can be calculated from eq 10 or 11. The key parameters are (i) the ratio of the surface area available for electron transfer reactions between the water (A_w) and organic (A_0) sides of the interface, (ii) the ratio of the nanofilm surface concentrations of the oxidized $[Fe(CN)_6]^{3-}$ species in the water phase ($c_{[Fe(CN)_6]^{3-}}^{w,s} \approx 10-100$ mM) and reduced Fc^0 species in the organic phase ($c_{Fc^o}^{o,s} \leq 0.1$ mM), and (iii) the ratio of standard rate constants for the water-based reduction (k_1^0) and oil-based oxidation (k_2^0) half-reactions at the nanofilm surface. As the apparent surface area available for linear semi-infinite diffusion of reactants toward the AuNP islands is roughly equal on both sides of the interface, the A_w/A_o ratio is close to unity. The kinetics of the $[Fe(CN)_6]^{3-/4-}$ electrode reactions are reasonably facile (k_1^0 = 0.04 cm s^{-1} on a gold electrode),[45] and Fc^0 oxidation is a model reversible reaction with facile kinetics; therefore $k_1^0/k_2^0 \approx 1$. Hence, the ratio $A_w k_1^0 c_{[Fe(CN)_6]^{3-}}^{w,s}/A_0 k_2^0 c_{Fc^o}^{o,s}$ in eq 11 is that of the concentrations of the redox species, *ca*. 100 to 1000, and E_F^{NP} will always be closer to E_F^w. In other words, the aqueous redox couple in excess pins the Fermi level on the gold NP nanofilm.

TABLE 1. Summary of the Experimentally Observed Values of Peak-to-Peak Separations (ΔE_p), Half-Wave Potentials ($\Delta_o^w\phi_{1/2}$), and i_{pf}/i_{pb} Ratios in Figure 3A and B (with Various Ratios between Fe^{2+} and Fe^{3+} Investigated for the Aqueous $[Fe(CN)_6]^{3-/4-}$ Redox Couple) at Both Bare and AuNP Nanofilm Functionalized Soft Interfaces

	bare soft interface			AuNP film functionalized soft interface		
$Fe^{2+/3+}$	ΔE_p/mV	$\Delta_o^w\phi_{1/2}$/mV	i_{pf}/i_{pb}	ΔE_p/mV	$\Delta_o^w\phi_{1/2}$/mV	i_{pf}/i_{pb}
10/100	93	206	1.4	66	207	1.1
55/55	90	275	1.0	66	275	0.9
100/10	135	330	1.4	71	330	0.9

An additional feature of the AuNP nanofilm is the increased cross-sectional area of the reaction: heterogeneous electron transfer across the interface requires that both reactants come close enough to each other to allow electron transfer from one molecule to the other. Hence, the rate of reaction also depends on the frequency of these encounters. However, with a gold island the electron donors and acceptors can charge and discharge the island upon contact. The latter increases the probability for electron transfer, as the AuNP islands provide a conductive interfacial route through which electrons can flow from the donor to acceptor molecules, circumventing the need for direct molecular encounters. Although the 30% coverage of the interface is probably not enough to allow electron conductivity through the whole film, there is local conductivity within the close-packed islands of NPs. This means that electrons injected into the film at the edge of the island can conduct through the island and be discharged at any point of contact.

CONCLUSIONS

We have presented a new theory based on Fermi level equilibration of two redox species in separate immiscible solutions, both in contact with an interfacial film of metallic nanoparticles, to understand interfacial redox catalysis, and this theory was used to explain the catalysis of interfacial heterogeneous electron transfer between the model redox couples $[Fe(CN)_6]^{3-/4-}$ in an aqueous phase and ferrocene/ferrocenium in an organic phase by gold nanoparticle islands. Additionally, a simple, reproducible, and scalable method of AuNP nanofilm sedimentation has been developed and implemented to create mirror-like films with controlled AuNP surface coverages. The AuNP nanofilm was characterized by ion transfer voltammetry of model species.

This work shows that electrochemistry at liquid–liquid interfaces is a powerful model system to study interfacial redox catalysis. Precise control of the Galvani potential difference between the two phases allows significant variation of the Fermi levels of electrons in aqueous and organic phases, resulting in direct

control of the rate and direction of electron transfer at a floating gold nanofilm adsorbed at the interface, highlighting the electrocatalytic properties of these films.

METHODS

Reagents. All chemicals were used as received without further purification. All aqueous solutions were prepared with ultrapure water (Millipore Milli-Q, specific resistivity 18.2MΩ·cm). Bis(triphenylphosphoranylidene)ammonium chloride (BACl, 98%), tetramethylammonium chloride (TMACl, 98%), tetrapropylammonium chloride (TPropACl, 98%), LiCl (>99%), dichlorodimethylsilane, and ferrocene (Fc, 98%) were purchased from Fluka. Hydrogen tetrachloroaurate(III) hydrate ($HAuCl_4 \cdot 3H_2O$, 99.999%, 49% Au) was provided by Alfa Aesar. Silver nitrate ($AgNO_3$, 99%) was bought from Chempur, and ascorbic acid ($C_6H_8O_6$) from Reidel-de-Haem. Trisodium citrate dihydrate ($Na_3C_6H_5O_7 \cdot 2H_2O$, 98%) and the organic solvent α,α,α-trifluorotoluene (99%+) were purchased from Acros. Bis(triphenylphosphoranylidene)ammonium tetrakis(pentafluorophenyl)borate (BATB) was prepared by metathesis of aqueous equimolar solutions of BACl and lithium tetrakis(pentafluorophenyl)borate ethyl etherate (LiTB-DEE purum, Boulder Scientific). The resulting precipitates were filtered, washed, and recrystallized from an acetone/methanol (1:1) mixture.

Preparation and Characterization of Gold Nanoparticles of Various Mean Diameters. In order to prepare AuNP suspensions with various mean diameters, a seed-growth method was selected.[46] This method is a two-step process involving synthesis of small, round-shape seeds followed by seed-mediated growth. The first step proceeds using a common procedure to prepare AuNPs.[47,48] Briefly, 41.5 mg of $HAuCl_4 \cdot 3H_2O$ was dissolved in 300 mL of deionized water in a round-bottomed flask with stirring, and the solution was heated to boiling point. A 9 mL amount of a 1% w/v trisodium citrate solution was then rapidly injected to form 13 (±1) nm AuNPs. In the second step, a solution containing 4 mL of 20 mM $HAuCl_4 \cdot 3H_2O$ and 0.4 mL of 10 mM $AgNO_3$ was prepared in 170 mL of deionized water. Next, 15 mL of the seed solution (prepared in the first step) was added. Finally, 30 mL of a 5 mM ascorbic acid solution was added in a dropwise manner under vigorous stirring using a syringe pump with a constant flow rate of 0.5 mL/min (60 min).

All AuNP suspensions were examined by UV/vis spectroscopy on a PerkinElmer Lambda XLS+ spectrophotometer with a 10 mm polystyrene cell in order to estimate the concentration of the AuNP suspensions in accordance with the work of Haiss *et al.*[40] Both Turkevich's[47,48] and Park's[46] methods reproducibly allow AuNP suspensions to be prepared with the desired AuNP concentrations. These were estimated as 4.0×10^9 particles/μL for 12 nm AuNPs and 1.1×10^8 particles/μL for 38 nm AuNPs. Particle size distributions for both sizes of AuNPs were obtained by two methods: DLS and TEM. The TEM images were recorded using a FEI CM12 (Phillips) transmission electron microscope, operating with a LaB_6 electron source at 120 kV. The size distributions of the AuNPs were estimated with ImageJ software from four to five individual images, gathering information from more than 150 particles. DLS measurements were performed with a Nano ZS Zetasizer (Malvern Instruments, U.K.), with irradiation (λ = 633 nm) from a He−Ne laser, using Dispersion Technology Software (DTS). The UV/vis spectroscopy, TEM, and DLS characterization data are presented in the Supporting Information, SI-1.

Modifying a Soft Interface with a Flat AuNP Nanofilm inside a Four-Electrode Electrochemical Cell. *Step (i): Preparing a Suspension of AuNPs in Methanol.* As-prepared solutions of citrate-stabilized AuNPs were centrifuged for 15 min in polypropylene tubes (at 8000 rpm for 12 nm AuNPs and 6000 rpm for 38 nm AuNPs). The supernatant was carefully decanted, leaving a highly concentrated aqueous solution of AuNPs with only *ca.* 0.1 mL of the initial 15 mL of solution remaining at the bottom of the plastic tube. A 0.2 mL amount of methanol was then added to the 0.1 mL solution of concentrated AuNPs. The concentrations were estimated by UV/vis spectroscopy as 1.5×10^{10} and 1×10^9 particles/μL for the 12 and 38 nm AuNPs, respectively.[40] Tightly sealed bottles of AuNP suspensions in methanol were stable for weeks.

Step (ii): Silanization of the Four-Electrode Electrochemical Cell. Prior to AuNP film preparation the electrochemical cell was silanized with dichlorodimethylsilane, as described previously.[49] Briefly, a certain volume (3.5 mL for the electrochemical cell modified herein) of a 10% (v/v) dichlorodimethylsilane/TFT solution was carefully injected underneath a layer of water in the electrochemical cell. The dichlorodimethylsilane/TFT solution volume was chosen such that the immiscible interface it forms with the top water layer was positioned midway between the two Luggin capillaries in the cell. The role of the water on top is to protect the top half of the electrochemical cell from becoming silanized. After 5 min, the dichlorodimethylsilane/TFT solution was carefully removed using a syringe and the glassware washed abundantly with acetone, ethanol, and deionized water. A hydrophobic protective layer was formed on the bottom half of the cell, preventing wetting of the glass by water and allowing the formation of a flat interface midway between the two Luggin capillaries.

Step (iii): Precise Microinjection of the AuNPs in Methanol at the Soft Interface. The AuNP methanol suspension was inserted into a 500 μL Hamilton syringe fixed in a syringe-pump. Next, a capillary (fused silica, inner diameter of 150 μm) was attached to

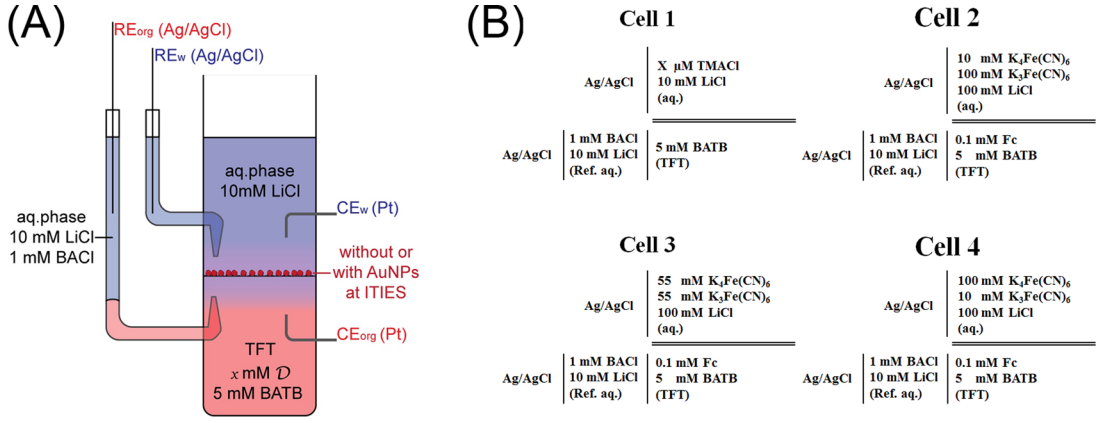

Scheme 4. (A) Scheme of the four-electrode electrochemical cell and (B) composition of the four-electrode electrochemical cells utilized in this study. 𝒟 denotes electron-donor molecules such as Fc.

the end of the syringe needle. The free end of the capillary was held in close proximity to the water | TFT interface in such a way that it only touched the interface by capillary forces. Finally, the syringe-pump was started and the gold nanofilm formation initiated. Varying the flow rate from 1 to 20 μL/min did not markedly influence the nanofilm formation process, and, thus, the flow rate was defined at 10 μL/min. A movie, the corresponding images, and a detailed explanation of the sedimentation process are provided in the Supporting Information, SI-2.

Determination of Redox Potential of Fc in TFT and $[Fe(CN)_6]^{3-/4-}$ in the Aqueous Phase. To determine the redox potentials of Fc in TFT, the electron transfer potential was measured between a 0.5 mM concentration of the donor molecule, Fc, in the oil phase and a mixture of $[Fe(CN)_6]^{3-/4-}$ in the aqueous phase. Next, the redox potential of $[Fe(CN)_6]^{3-/4-}$ was evaluated with ultramicroelectrode voltammetry (d_{Pt} = 25 μm, RG (radius of the tip divided by the radius of the Pt disc in the center of the tip) = 6.15) in a 100 mM solution of both $[Fe(CN)_6]^{3-}$ and $[Fe(CN)_6]^{4-}$ with 100 mM LiCl as the supporting electrolyte. A complete description of the experimental approach is presented in the Supporting Information, SI-5.

Ion and Electron Transfer Voltammetry. All IT and ET voltammetry measurements at the water | TFT interface were performed using a four-electrode cell following the configuration described previously by Hatay *et al.*[50] and illustrated in Scheme 4A. The different electrochemical cells investigated in this study are outlined in detail in Scheme 4B.

Briefly, two platinum electrodes provide current and potential difference, whereas two pseudoreference Ag/AgCl electrodes allow measurement and correction of the polarization across the interface. TFT was chosen as the solvent, as the water | TFT interface provides a larger window and is chemically both more stable and less toxic in comparison to chlorinated organic solvents.[51] Commercially available potentiostats, PGSTAT 30 and PGSTAT 101 (Metrohm, Switzerland), were used. The Galvani potential difference, in accordance with the TATB assumption,[52] was calibrated by addition of internal standards TMA^+ and $TProA^+$ ions, whose $\Delta_o^w\phi_{1/2}$ at the water | TFT interface were taken to be +0.270 V for TMA^+ and −0.019 V for $TProA^+$, respectively.[51,53] For all experiments 10 mM LiCl and 5 mM BATB were chosen as the aqueous and oil phase background electrolytes, respectively, and used to maintain electrical conductance. The organic reference solution (see Scheme 4) was 10 mM LiCl and 1 mM BACl in water.

Conflict of Interest: The authors declare no competing financial interest.

Supporting Information Available: Supporting movie on sedimentation process as well as snapshots, characterization by TEM, SEM, UV/spectroscopy, and DLS measurements, determination of standard redox potential and control experiments, and overview of electrochemical analysis. The Supporting Information is available free of charge on the ACS Publications website at DOI: 10.1021/acsnano.5b02547.

Acknowledgment. We would like to acknowledge financial support from Fondazione Oronzio e Niccolò De Nora, Swiss National Science Foundation, and the Swiss Federal Office of Energy. This publication has emanated from research by M.D.S. supported in part by a research grant from Science Foundation Ireland (SFI) under Grant No. 13/SIRG/2137.

REFERENCES AND NOTES

1. Reymond, F.; Fermin, D. J.; Lee, H. J.; Girault, H. H. Electrochemistry at Liquid/liquid Interfaces: Methodology and Potential Applications. *Electrochim. Acta* **2000**, *45*, 2647–2662.
2. Hatay, I.; Su, B.; Li, F.; Partovi-Nia, R.; Vrubel, H.; Hu, X.; Ersoz, M.; Girault, H. H. Hydrogen Evolution at Liquid-Liquid Interfaces. *Angew. Chem.* **2009**, *48*, 5139–5142.
3. Scanlon, M. D.; Bian, X.; Vrubel, H.; Amstutz, V.; Schenk, K.; Hu, X.; Liu, B.; Girault, H. H. Low-Cost Industrially Available Molybdenum Boride and Carbide as "Platinum-like" Catalysts for the Hydrogen Evolution Reaction in Biphasic Liquid Systems. *Phys. Chem. Chem. Phys.* **2013**, *15*, 2847–2857.
4. Ge, P.; Scanlon, M. D.; Peljo, P.; Bian, X.; Vubrel, H.; O'Neill, A.; Coleman, J. N.; Cantoni, M.; Hu, X.; Kontturi, K.; Liu, B.; Girault, H. H. Hydrogen Evolution across Nano-Schottky Junctions at Carbon Supported MoS_2 Catalysts in Biphasic Liquid Systems. *Chem. Commun.* **2012**, *48*, 6484–6486.
5. Adamiak, W.; Jedraszko, J.; Krysiak, O.; Nogala, W.; Hidalgo-Acosta, J. C.; Girault, H. H.; Opallo, M. Hydrogen and Hydrogen Peroxide Formation in Trifluorotoluene–Water Biphasic Systems. *J. Phys. Chem. C* **2014**, *118*, 23154–23161.
6. Peljo, P.; Murtomäki, L.; Kallio, T.; Xu, H.-J.; Meyer, M.; Gros, C. P.; Barbe, J.-M.; Girault, H. H.; Laasonen, K.; Kontturi, K. Biomimetic Oxygen Reduction by Cofacial Porphyrins at a Liquid-Liquid Interface. *J. Am. Chem. Soc.* **2012**, *134*, 5974–5984.
7. Su, B.; Hatay, I.; Trojánek, A.; Samec, Z.; Khoury, T.; Gros, C. P.; Barbe, J.-M.; Daina, A.; Carrupt, P.-A.; Girault, H. H. Molecular Electrocatalysis for Oxygen Reduction by Cobalt Porphyrins Adsorbed at Liquid/liquid Interfaces. *J. Am. Chem. Soc.* **2010**, *132*, 2655–2662.
8. Olaya, A. A. J.; Schaming, D.; Brevet, P.-F.; Nagatani, H.; Zimmermann, T.; Vanicek, J.; Xu, H.-J.; Gros, C. P.; Barbe, J.-M.; Girault, H. H. Self-Assembled Molecular Rafts at Liquid|Liquid Interfaces for Four-Electron Oxygen Reduction. *J. Am. Chem. Soc.* **2012**, *134*, 498–506.
9. Trojánek, A.; Langmaier, J.; Samec, Z. Electrocatalysis of the Oxygen Reduction at a Polarised Interface between Two Immiscible Electrolyte Solutions by Electrochemically Generated Pt Particles. *Electrochem. Commun.* **2006**, *8*, 475–481.
10. Rastgar, S.; Deng, H.; Cortés-Salazar, F.; Scanlon, M. D.; Pribil, M.; Amstutz, V.; Karyakin, A. A.; Shahrokhian, S.; Girault, H. H. Oxygen Reduction at Soft Interfaces Catalyzed by in Situ-Generated Reduced Graphene Oxide. *ChemElectroChem* **2014**, *1*, 59–63.
11. Hatay Patir, I. Oxygen Reduction Catalyzed by Aniline Derivatives at Liquid/Liquid Interfaces. *J. Electroanal. Chem.* **2012**, *685*, 28–32.
12. Binder, W. H. Supramolecular Assembly of Nanoparticles at Liquid-Liquid Interfaces. *Angew. Chem.* **2005**, *44*, 5172–5175.
13. Edel, J. B.; Kornyshev, A. a; Urbakh, M. Self-Assembly of Nanoparticle Arrays for Use as Mirrors, Sensors, and Antennas. *ACS Nano* **2013**, *7*, 9526–9532.
14. Yogev, D.; Efrima, S. Novel Silver Metal Liquidlike Films. *J. Phys. Chem.* **1988**, *92*, 5754–5760.
15. Turek, V. A.; Cecchini, M. P.; Paget, J.; Kucernak, A. R.; Kornyshev, A. A.; Edel, J. B. Plasmonic Ruler at the Liquid-Liquid Interface. *ACS Nano* **2012**, *6*, 7789–7799.
16. Smirnov, E.; Scanlon, M. D.; Momotenko, D.; Vrubel, H.; Méndez, M. A.; Brevet, P.-F.; Girault, H. H. Gold Metal Liquid-Like Droplets. *ACS Nano* **2014**, *8*, 9471–9481.
17. Duan, H.; Wang, D.; Kurth, D. G.; Mohwald, H. Directing Self-Assembly of Nanoparticles at Water/Oil Interfaces. *Angew. Chem.* **2004**, *116*, 5757–5760.
18. Rao, C. N. R.; Kalyanikutty, K. P. The Liquid-Liquid Interface as a Medium to Generate Nanocrystalline Films of Inorganic Materials. *Acc. Chem. Res.* **2008**, *41*, 489–499.
19. Fang, P.-P.; Chen, S.; Deng, H.; Scanlon, M. D.; Gumy, F.; Lee, H. J.; Momotenko, D.; Amstutz, V.; Cortes-Salazar, F.; Pereira, C. M.; Yang, Z.; Girault, H. H. Conductive Gold Nanoparticle Mirrors at Liquid/Liquid Interfaces. *ACS Nano* **2013**, *7*, 9241–9248.
20. Cecchini, M. P.; Turek, V. A.; Paget, J.; Kornyshev, A. A.; Edel, J. B. Self-Assembled Nanoparticle Arrays for Multiphase Trace Analyte Detection. *Nat. Mater.* **2012**, *12*, 165–171.
21. Zhang, K.; Ji, J.; Li, Y.; Liu, B. Interfacial Self-Assembled Functional Nanoparticle Array: A Facile Surface-Enhanced Raman Scattering Sensor for Specific Detection of Trace Analytes. *Anal. Chem.* **2014**, *86*, 6660–6665.
22. Kowalczyk, B.; Lagzi, I.; Grzybowski, B. A. Nanoarmoured" Droplets of Different Shapes Formed by Interfacial

Self-Assembly and Crosslinking of Metal Nanoparticles. *Nanoscale* **2010**, *2*, 2366–2369.
23. Daniel, M. C.; Astruc, D. Gold Nanoparticles: Assembly, Supramolecular Chemistry, Quantum-Size-Related Properties, and Applications toward Biology, Catalysis, and Nanotechnology. *Chem. Rev.* **2004**, *104*, 293–346.
24. Reincke, F.; Hickey, S. G.; Kegel, W. K.; Vanmaekelbergh, D. Spontaneous Assembly of a Monolayer of Charged Gold Nanocrystals at the Water/Oil Interface. *Angew. Chem.* **2004**, *43*, 458–462.
25. Peng, L.; You, M.; Wu, C.; Han, D.; Öçsoy, I.; Chen, T.; Chen, Z.; Tan, W. Reversible Phase Transfer of Nanoparticles Based on Photoswitchable Host-Guest Chemistry. *ACS Nano* **2014**, *8*, 2555–2561.
26. Liu, Y.; Han, X.; He, L.; Yin, Y. Thermoresponsive Assembly of Charged Gold Nanoparticles and Their Reversible Tuning of Plasmon Coupling. *Angew. Chem.* **2012**, *51*, 6373–6377.
27. Younan, N.; Hojeij, M.; Ribeaucourt, L.; Girault, H. H. Electrochemical Properties of Gold Nanoparticles Assembly at Polarised Liquid|Liquid Interfaces. *Electrochem. Commun.* **2010**, *12*, 912–915.
28. Park, Y.-K.; Yoo, S.-H.; Park, S. Assembly of Highly Ordered Nanoparticle Monolayers at a Water/Hexane Interface. *Langmuir* **2007**, *23*, 10505–10510.
29. Schaming, D.; Hojeij, M.; Younan, N.; Nagatani, H.; Lee, H. J.; Girault, H. H. Photocurrents at Polarized Liquid|Liquid Interfaces Enhanced by a Gold Nanoparticle Film. *Phys. Chem. Chem. Phys.* **2011**, *13*, 17704–17711.
30. Scanlon, M. D.; Peljo, P.; Mendez, M. A.; Smirnov, E.; Girault, H. Charging and Discharging at the Nanoscale: Fermi Level Equilibration of Metallic Nanoparticles. *Chem. Sci.* **2015**, *6*, 2705–2720.
31. Novo, C.; Funston, A. M.; Mulvaney, P. Direct Observation of Chemical Reactions on Single Gold Nanocrystals Using Surface Plasmon Spectroscopy. *Nat. Nanotechnol.* **2008**, *3*, 598–602.
32. Kleijn, S. E. F.; Lai, S. C. S.; Koper, M. T. M.; Unwin, P. R. Electrochemistry of Nanoparticles. *Angew. Chem.* **2014**, *53*, 3558–3586.
33. Su, B.; Nia, R. P.; Li, F.; Hojeij, M.; Prudent, M.; Corminboeuf, C.; Samec, Z.; Girault, H. H. H_2O_2 Generation by Decamethylferrocene at a Liquid|Liquid Interface. *Angew. Chem.* **2008**, *47*, 4675–4678.
34. Nieminen, J. J.; Hatay, I.; Ge, P.-Y. P.; Méndez, M. A.; Murtomäki, L.; Girault, H. H. Hydrogen Evolution Catalyzed by Electrodeposited Nanoparticles at the Liquid/Liquid Interface. *Chem. Commun.* **2011**, *47*, 5548–5550.
35. Girault, H. H.; Peljo, P. Liquid/Liquid Interfaces, Electrochemistry at. In *Encyclopedia of Analytical Chemistry*; Meyers, R. A., Ed.; John Wiley & Sons, Inc.: New York, 2012; pp 1−28.
36. Samec, Z.; Mareček, V.; Weber, J. Charge Transfer between Two Immiscible Electrolyte Solutions. *J. Electroanal. Chem. Interfacial Electrochem.* **1979**, *103*, 11–18.
37. Kihara, S.; Suzuki, M.; Maeda, K.; Ogura, K.; Matsui, M.; Yoshida, Z. The Electron Transfer at a Liquid/Liquid Interface Studied by Current-Scan Polarography at the Electrolyte Dropping Electrode. *J. Electroanal. Chem.* **1989**, *271*, 107–125.
38. Hotta, H.; Ichikawa, S.; Sugihara, T.; Osakai, T. Clarification of the Mechanism of Interfacial Electron-Transfer Reaction between Ferrocene and Hexacyanoferrate(III) by Digital Simulation of Cyclic Voltammograms. *J. Phys. Chem. B* **2003**, *107*, 9717–9725.
39. Tatsumi, H.; Katano, H. Cyclic Voltammetry of the Electron Transfer Reaction between Bis(cyclopentadienyl)iron in 1,2-Dichloroethane and Hexacyanoferrate in Water. *Anal. Sci.* **2007**, *23*, 589–591.
40. Haiss, W.; Thanh, N. T. K.; Aveyard, J.; Fernig, D. G. Determination of Size and Concentration of Gold Nanoparticles from UV-Vis Spectra. *Anal. Chem.* **2007**, *79*, 4215–4221.
41. Amatore, C.; Savéant, J. M.; Tessier, D. Charge Transfer at Partially Blocked Surfaces. *J. Electroanal. Chem.* **1983**, *147*, 39–51.
42. Davies, T. J.; Compton, R. G. The Cyclic and Linear Sweep Voltammetry of Regular and Random Arrays of Microdisc Electrodes: Theory. *J. Electroanal. Chem.* **2005**, *585*, 63–82.
43. Bard, A. J.; Faulkner, L. R. *Electrochemical Methods: Fundamentals and Applications*, 2nd ed.; John Wiley & Sons Inc.: New York, 2001.
44. Volkov, A. G. *Interfacial Catalysis*; Marcel Dekker, Inc.: New York, 2003.
45. Mareček, V.; Samec, Z.; Weber, J. The Dependence of the Electrochemical Charge-Transfer Coefficient on the Electrode Potential. *J. Electroanal. Chem.* **1978**, *94*, 169–185.
46. Park, Y.-K.; Park, S. Directing Close-Packing of Midnanosized Gold Nanoparticles at a Water/Hexane Interface. *Chem. Mater.* **2008**, *20*, 2388–2393.
47. Turkevich, J.; Stevenson, P. C.; Hillie, J. A Study of the Nucleation and Growth Processes in the Sythesis of Colloidal Gold. *Discuss. Faraday Soc.* **1951**, *11*, 75–82.
48. Frens, G. Controlled Nucleation for the Regulation of the Particle Size in Monodisperse Gold Suspensions. *Nat. Phys. Sci.* **1973**, *241*, 20.
49. Seed, B. Silanizing Glassware. In *Current Protocols in Immunology*; Coico, R., Ed.; John Wiley & Sons, Inc.: New York, 1997; pp A3.K1−A3.K2.
50. Hatay, I.; Su, B.; Li, F.; Méndez, M. A.; Khoury, T.; Gros, C. P.; Barbe, J.-M.; Ersoz, M.; Samec, Z.; Girault, H. H. Proton-Coupled Oxygen Reduction at Liquid-Liquid Interfaces Catalyzed by Cobalt Porphine. *J. Am. Chem. Soc.* **2009**, *131*, 13453–13459.
51. Olaya, A. A. J.; Ge, P.-Y.; Girault, H. H. Ion Transfer across the Water|Trifluorotoluene Interface. *Electrochem. Commun.* **2012**, *19*, 101–104.
52. Wilke, S.; Zerihun, T. Standard Gibbs Energies of Ion Transfer across the Water|2-Nitrophenyl Octyl Ether Interface. *J. Electroanal. Chem.* **2001**, *515*, 611–614.
53. ElectroChemical DataBase: Gibbs Energies of transfer, http://sbsrv7.epfl.ch/instituts/isic/lepa/cgi/DB/InterrDB.pl.